

26. MAGNETOSTRATIGRAPHY OF LEG 108 ADVANCED HYDRAULIC PISTON CORES¹

Lisa Tauxe,² Jean-Pierre Valet,³ and Jan Bloemendal⁴

ABSTRACT

This paper presents the magnetostratigraphic results from Leg 108 of the Ocean Drilling Program. Measurements made with the shipboard "pass-through" cryogenic magnetometer on whole cores and archive halves are combined with those made on discrete samples; these measurements constitute the paleomagnetic data base for the Leg 108 cores. Polarity determination on unoriented, low-latitude cores is somewhat subjective; we rely heavily on the available biostratigraphic data and document our line of reasoning where appropriate. The interpretations presented here, therefore, are compatible with the available biostratigraphic information; they are also in substantial agreement with orientation information where available.

INTRODUCTION

Since the early days of deep-sea coring, magnetostratigraphic data have proved useful for the correlation of sedimentary records and for precise calibration with respect to time (e.g., Theyer and Hammond, 1974; Hays et al., 1969; Opdyke et al., 1974). The use of the hydraulic piston corer (HPC), superseded by the advanced hydraulic piston corer (APC) since Leg 64 of the Deep Sea Drilling Project (DSDP), allowed the recovery of undisturbed sediments from unprecedented depths.

Other technological developments, such as the introduction of a three-axis, "pass-through" cryogenic magnetometer on board the *JOIDES Resolution*, have eased the rapid and nearly continuous measurement of core material with minimal subsampling and associated degradation of core material. We present here the magnetostratigraphic results from Leg 108 APC cores based largely on shipboard measurements of archive halves. These data, when combined with the available biostratigraphic data, provide a rather tight chronostratigraphic framework for interpreting sediment accumulation rates discussed elsewhere.

METHODS

The paleomagnetic laboratory on board the ship features two magnetometers: a 2G Enterprises three-axis cryogenic magnetometer with a through-bore sample access tube and a Molspin "Minispin" magnetometer. The former has been automated to allow rapid measurement of entire cores as frequently as 2-cm intervals. The latter is primarily useful for measuring standard 8–10-cm³ paleomagnetic specimens subsampled from the core. An alternating-field (AF) demagnetizer is mounted onto the 2G magnetometer track (peak field of about 9 mT) for use on whole-core sections. Discrete specimens may be demagnetized with a Schonstedt Instruments single-axis AF demagnetizer (peak field of 100 mT).

Calibration specimens brought from the Scripps Paleomagnetic Laboratory demonstrated excellent cross-laboratory agreement; the minispin and the cryogenic were also cross-calibrated. The noise level of both magnetometers was about 10⁻⁹ Am² (total moment). Similar shore-based cryogenics have noise levels several orders of magnitude

lower. The unusually high noise level on the shipboard cryogenic is due to the motion of the ship itself. Despite the relatively high noise level, the volume of material represented by using an entire core section (or even the archive half) is such that all the material recovered was easily measurable.

In general, our procedure was as follows. Either the whole core or the archive half was measured from 3- to 5-cm intervals. The maximum demagnetizing field allowed by the curatorial staff was 5 mT, and all cores were demagnetized to this level. Data were discarded from within 3 cm of a core section edge as well as from portions of the cores that suffered drilling disturbance or slumping. Certain turbidite units were associated with scattered remanent directions (particularly at Site 666); these were also deleted when appropriate. However, we were careful not to "overedit" in order to preserve the true nature of the record.

Our whole-core measurements have not been deconvolved. The *x*, *y*, and *z* measurements were converted to relative declination, inclination, and intensity by assuming an "effective volume" for each axis. The units of our intensity data are therefore a nominal 10⁻² mA/m. The volume normalization factor was estimated from the shapes of curves obtained by measuring a calibration specimen (assumed to be a point source). For a 3-cm spacing, then, the data points are not independent of their neighbors and some smoothing is inevitable. However, we have validated the use of this approximation by comparing data from whole-core measurements with those obtained from closely spaced (0.5 cm) discrete samples and found the correspondence to be excellent (see Fig. 1). Also shown in Figure 1 are data from an instrument at Scripps (identical to the shipboard instrument) obtained from a 2- × 2- × 50-cm "U" channel subsample of the same core. We find the agreement to be encouraging.

Discrete samples obtained from the working half of the core (generally one per section) were measured either on the minispin or on the cryogenic. Where possible, one specimen per core was subjected to stepwise AF demagnetization in order to determine the stability of remanence and the level of demagnetization necessary to isolate the characteristic remanence. Based on these demagnetization curves, the remaining specimens were demagnetized to the appropriate level (usually 10–20 mT). All data plotted for magnetostratigraphic interpretation were selected as follows: (1) the intensity must be above the noise level of the instrument, (2) the circular standard deviation for the measurement must be below 35°, and (3) the specimen must be demagnetized to the level deemed appropriate based on stepwise demagnetization data from the pilot specimens. All the discrete sample data plotted for magnetostratigraphic interpretation are derived from demagnetization to a single step.

We hoped that oriented cores could be obtained for the equatorial sites. A multishot photographic core orientation device was available for this purpose, but a lack of time and insufficient battery power precluded its use for every core. With the exception of a few holes, the cores were unoriented. For the higher latitude sites (657, 658, and 659), we relied on the inclinations of cleaned discrete samples as an

¹ Ruddiman, W., Sarnthein, M., et al., 1989. *Proc. ODP, Sci. Results*, 108: College Station, TX (Ocean Drilling Program).

² Scripps Institution of Oceanography, La Jolla, CA 92093.

³ Centre des Faibles Radioactivités, Laboratoire Mixte CNRS-CEA, Parc du CNRS, B. P. 91198, Gif/Yvette Cedex, France.

⁴ Graduate School of Oceanography, University of Rhode Island, Narragansett, RI 02882-1197.

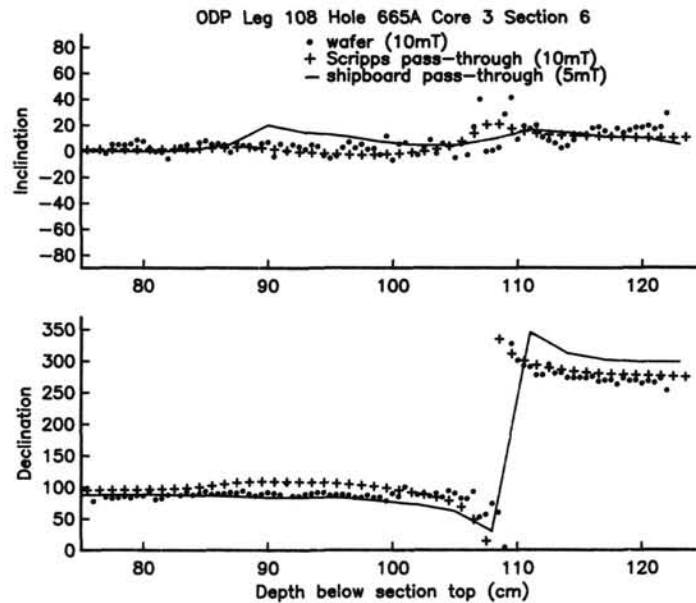


Figure 1. Comparison of shipboard 2G Enterprises pass-through magnetometer (solid line) and shore-based measurements. A 2- × 2- × 50-cm "U" channel was taken out of the working half of the core and measured using an identical instrument housed in the Scripps Paleomagnetic Laboratory (plus signs). The "U" channel sample was then sliced into 0.5-cm wafers and measured using a CTF cryogenic magnetometer, also at Scripps (closed circles). The data indicate the high degree of reliability of the shipboard instrument.

indication of polarity. At the equatorial sites, however, polarity picks were somewhat more subjective. Because of the generally good recovery and the 9-m length of the core, many polarity boundaries occurred within a single core, as opposed to between cores. These two types of boundaries are distinguished in the polarity logs for the purposes of clarity. By using the excellent biostratigraphic data (particularly the nannofossil data), polarity boundaries could often be uniquely identified.

At times, magnetic behavior during demagnetization can also give clues as to polarity. If an overprint was acquired in the present field, its removal resulted in an increase in intensity during early demagnetization. Although this is not a universally reliable technique, such data may be used to support suspicions based on other criteria (multishot data, inclinations, and biostratigraphy). After assigning polarity to the core data, a single declination correction was applied to each core such that the average "normal" declination was approximately zero. In this way, a magnetostratigraphic record could be constructed that was consistent with the available biostratigraphic information.

Because of the length of the APC cores and the excellent recovery in many holes, we think that the results presented here are quite reliable, although other interpretations are certainly possible. We have tried to present all the data so that the reader may reinterpret data as necessary. In general, we have only identified major polarity intervals (chrons and the Jaramillo and Olduvai Subchrons). These are assigned ages using the time scale of Berggren et al. (1985) for consistency with the rest of the volume. Some of the shorter wavelength features undoubtedly reflect field behavior; but without substantial subsampling and detailed demagnetization data, we cannot place much confidence in their interpretation.

Because of problems with overprinting (discussed later), we have taken a conservative approach; the data are provided, however, and may be interpreted as the reader sees fit. Although crucial to the

understanding of sedimentary paleomagnetism, we will not discuss any aspects of the magnetic mineralogy. These studies will be presented elsewhere (Valet et al., this volume; Bloemendal et al., this volume).

RESULTS

Demagnetization Behavior

In Figure 2 we plotted demagnetization diagrams that are representative of the range of behavior displayed by Leg 108 sediments. Figure 2 illustrates the best of our normal (A) and reversely magnetized (B) specimens. The demagnetization behavior (here called Type I) is linear and the median destructive field is between 20 and 30 mT, indicating a high stability of remanence. The expected inclinations for the sites (assuming an axial geocentric dipole) were 38° (normal) and -38° (reversed), in close agreement with those observed.

A second common behavior (Type II) is illustrated in Figures 2C and 2D. These show a nearly vertical overprint of varying stability. A normal inclination is isolated in Figure 2C by 10 mT, whereas the reversed character of the specimen shown in Figure 2D is not evident until 16 mT. The origin of this vertical component is presumably related to the coring process in some way since the present field is almost horizontal at the equatorial sites; but whether it is viscous, isothermal, or some kind of physical reorientation is unknown. It can be quite stable, in some cases, and results in a complete overprint of many sections of pre-Matuyama age.

In Figure 2E we show a specimen with a linear demagnetization trajectory but with a median destructive field of less

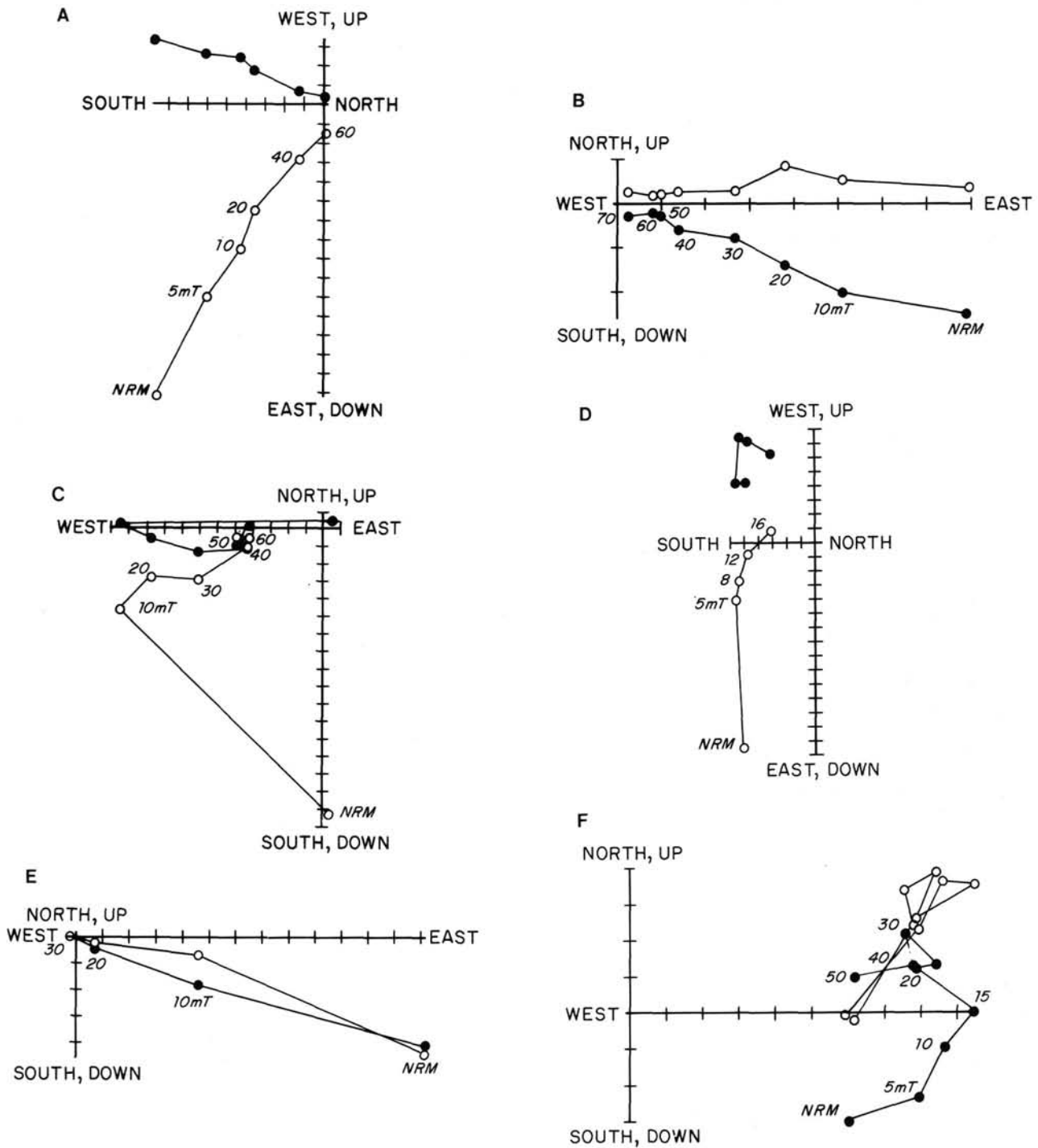


Figure 2. Representative behavior of Leg 108 sediments during stepwise alternating-field demagnetization. Solid symbols are the projection of the vector onto the horizontal plane, while open symbols are projections onto either the x-z or y-z vertical plane. The declinations have not been corrected and are azimuthally unoriented. A. Section 108-657A-11H-1, 96-98 cm. B. Section 108-667A-2H-3, 60-62 cm. C. Section 108-665B-3H-5, 30-32 cm. D. Section 108-659C-4H-3, 38-40 cm. E. Section 108-667A-3H-2, 60-62 cm. F. Section 108-657A-7H-6, 111-113 cm. Intensity units of all samples are in 10^{-3} Am^2 with the exception of A, E, and F, which are 10^{-4} Am^2 .

Table 1. Depths to chron and subchron boundaries (to the nearest decimeter).

Site and time zone	Depth (mbsf)	Core, section, interval (cm)
108-657B		
Brunhes/Matuyama	29.0	4H-5, 130
Jaramillo (upper)	30.7–34.7	4H-6, 140/5H-1, 50
Jaramillo (lower)	36.2	5H-4, 50
Matuyama/Gauss	72.1–73.7	9H-2, 140/9H-4, 2
108-658A		
Brunhes/Matuyama	—	—
(Unconfirmed?)	100.6–103.8	11H-7, 40/12H-3, 10
Olduvai (upper)	109.2–109.8	12H-6, 102/12H-7, 10
Olduvai (lower)	124.1–129.7	14H-3, 140/15H-1, 50
108-658B		
(Unconfirmed?)	100.5–103.0	11H-9, 71/12H-4, 121
Olduvai (upper)	108.2	12H-8, 41
Olduvai (lower)	126.2	14H-7, 91
108-659A		
Brunhes/Matuyama	22.8	3H-4, 100
Jaramillo (upper)	28.6	4H-2, 30
Jaramillo (lower)	31.0	4H-3, 120
108-659B		
Brunhes/Matuyama	—	—
Jaramillo (upper)	26.4	4H-1, 80
Jaramillo (lower)	29.3	4H-3, 70
Olduvai (upper)	47.8	6H-3, 22
Olduvai (lower)	52.4	6H-6, 30
Matuyama/Gauss	74.7	9H-2, 10
108-660A		
Brunhes/Matuyama	18.5	3H-5, 120
Jaramillo (upper)	22.9	4H-2, 60
Jaramillo (lower)	24.6	4H-3, 80
Olduvai (upper)	36.4	5H-5, 10
Olduvai (lower)	38.4	5H-6, 60
108-661A		
Brunhes/Matuyama	10.5–12.7	2H-6, 140/3H-2, 10
Jaramillo (upper)	14.8	3H-3, 70
Jaramillo (lower)	16.0	3H-4, 40
Olduvai (upper)	26.1–26.7	5H-2, 40
Matuyama/Gauss	36.8	5H-5, 70
108-661B		
Brunhes/Matuyama	13.1–15.7	2H-5, 140/3H-1, 50
Jaramillo (upper)	—	—
Jaramillo (lower)	—	—
Olduvai (upper)	25.4	4H-1, 70
Olduvai (lower)	30.2	4H-4, 100
Matuyama/Gauss	36.2	5H-2, 50
Gauss/Gilbert	52.5	6H-6, 130
108-664B		
Brunhes/Matuyama	27.0	3H-6, 50
Jaramillo (upper)	35.5	4H-5, 100
108-664C		
Brunhes/Matuyama	25.9	4H-2, 120
Jaramillo (upper)	34.5	5H-2, 30
Jaramillo (lower)	37.6	5H-4, 40
108-664D		
Brunhes/Matuyama	27.9	4H-5, 59
Jaramillo (upper)	35.8	5H-4, 50
Jaramillo (lower)	38.2	5H-5, 140
108-665A		
Brunhes/Matuyama	14.8	3H-2, 90
Jaramillo (upper)	19.3	3H-5, 90
Jaramillo (lower)	21.0	3H-6, 110
Olduvai (upper)	33.2	5H-2, 30
Olduvai (lower)	36.4	5H-4, 50
Matuyama/Gauss	49.1	6H-6, 70
108-665B		
Brunhes/Matuyama	13.8	2H-6, 30
Jaramillo (upper)	16.9	3H-1, 140
Jaramillo (lower)	18.7	3H-3, 20
Olduvai (upper)	32.6	4H-6, 10
Olduvai (lower)	34.3–35.0	4H-7, 30/4H-7, 50
Matuyama/Gauss	49.1	6H-4, 60

Table 1 (continued).

Site and time zone	Depth (mbsf)	Core, section, interval (cm)
108-666A		
Brunhes/Matuyama	18.4	3H-1, 90
Olduvai (upper)	34.4–37.1	4H-5, 140/5H-1, 60
Olduvai (lower)	45.0	5H-6, 100
Matuyama/Gauss	77.6	9H-3, 10
108-668B		
Brunhes/Matuyama	12.1–15.3	2H-7, 40/3H-3, 10
Olduvai (upper)	27.6	4H-4, 140
Olduvai (lower)	29.8	4H-6, 60

than 10 mT. Such data (Type III) are suspect owing to the low stability of remanence. Occasionally, behavior such as that shown in Figure 2F was observed (Type IV). Whereas the polarity of the specimen is likely to be reversed, the magnetization can hardly be characterized as simple. Therefore, data from such specimens are viewed with caution.

Magnetostratigraphy

Magnetostratigraphic results are shown in Figures 3–20. We list the reversal boundaries to the nearest decimeter in Table 1. Reversal boundaries contained within a single core are indicated by a straight line in the polarity log, whereas those inferred to lie between cores are indicated by ragged lines. Gaps are shown as hachured areas. Each hole presented slightly different problems; therefore, we will discuss the results from each site separately.

Site 657

Unlike most of the other sites, Site 657 was plagued by poor core recovery. Whole cores were measured at 5-cm intervals. Results from Hole 657B are shown in Figure 3. Despite poor core recovery, several reversals were detected within a single core: the Brunhes/Matuyama (B/M) at 29 meters below the sea-floor (mbsf), the lower Jaramillo at 36.2 mbsf, and the Matuyama/Gauss (M/Ga) at 72.3 mbsf. Since the site was located at 21°N, the expected inclination ($\pm 38^\circ$) was sufficient to determine the polarity of cleaned specimens. One discrete sample per core section was measured and demagnetized to between 10 and 20 mT (a total of about 100 samples). Above about 60 mbsf, inclinations measured on the discrete samples were close to the expected value. Below this, the positive inclinations were too steep and the negative inclinations, too shallow; below about 80 mbsf the data were apparently completely overprinted.

Site 658

Whole cores from Hole 658A were measured at 5-cm intervals, and those from 658B at 10-cm intervals. A total of approximately 200 discrete samples were also measured. In most cases, the demagnetization behavior was Type I. An AF demagnetization of 5 mT was sufficient to isolate those characteristic directions with inclinations in close agreement with expected values ($\pm 37^\circ$). The combined whole-core and discrete sample results are shown in Figures 4 and 5. Above about 110 mbsf, the agreement between discrete and whole-core measurements is quite remarkable; below that depth, the whole-core inclinations are somewhat larger, but they are still unambiguous as to polarity. No boundaries were recovered within a single core at Hole 658A, but polarity interpretations could be based on the inclination data. The identification of the Olduvai (O_u-O_l) Subchron (~ 109 – 127 mbsf) is based on biostratigraphic data (last appearance datum of *Discoaster brouweri*).

At Hole 658B, both upper and lower boundaries of the Olduvai were recovered (~108–126 mbsf). The B/M boundary was recovered at neither hole, and we suspect it was removed by an unconformity. Below about 160 mbsf, cores were taken with the extended core barrel (XCB), and whole-core measurements were highly scattered. Discrete sample inclinations were far steeper than the expected values (50°–75°); hence, these data are considered unreliable.

Site 659

For the most part, archive sections were measured at 3-cm intervals; however, the first four cores at Hole 659A were measured before splitting. Some 1500 discrete samples were measured, although the directions below about 100 mbsf are highly scattered. We show the reliable data in Figures 6 and 7. The fact that the B/M as well as the upper Jaramillo (J_u) and the lower Jaramillo (J_l) were recovered at Site 659A, as well as the high expected inclination of 33°, makes the polarity identifications at this hole particularly reliable. At Hole 659B, both boundaries of the Jaramillo and the Olduvai were recovered, although the data from the latter are quite scattered. The Matuyama/Gauss (M/Ga) boundary was also recovered from Hole 659B. We attribute the increasing scatter and a steepening of directions downhole to incomplete removal of a hard vertical overprint.

The remanent intensity is relatively high in the upper part of the sequence. It drops to very low values below the Jaramillo and then rises again in the Gauss (where the sediments also turn reddish). The steep inclinations are particularly common in the high-intensity, Gauss-aged part of the record, as frequently noted during Leg 108.

Site 660

Archive sections were measured at 3-cm intervals. Despite the shallow expected inclinations (19°), demagnetized data from discrete samples could be used to determine polarity with reasonable confidence above about 50 mbsf. Below 50 mbsf there was little agreement between the whole-core and discrete sample measurements, rendering them suspect. In Figure 8 we show the results above 50 mbsf. Please note the excellent agreement between the two data sets. The B/M, J_u , J_l , and M/Ga boundaries were all retrieved within single cores, making this a highly successful site.

Site 661

The results from Site 661 are shown in Figures 9 and 10. Archive sections were measured at 3-cm intervals, and many discrete specimens supplement the data set. The expected inclination for the site is about 19°, which is sufficient for unique polarity determination using cleaned data. Incomplete removal of a steep secondary overprint is indicated by the consistent difference between the whole-core and the discrete sample data sets. Despite the offset, polarities are unambiguous and the O_u , O_l , and M/Ga boundaries were recovered in both holes. The J_u and J_l boundaries were recovered in Hole 661A, but the B/M boundary was missed in both holes. The Gauss/Gilbert (Ga/Gi) boundary was also recovered from Hole 661B. Data below about 50 mbsf displayed a post-splitting remanence, evident from measuring archive and working halves (which were identically magnetized, rather than in a mirror image as required). Also, there was no agreement between whole-core and subsample measurements. However, the data above 50 mbsf may be considered quite reliable.

Sites 662 and 663

No reliable measurements were obtained from these sites. Identical data from the archive and working halves suggest excessive grain mobility, and no reliable record survived coring. Owing to the extremely weak magnetization, no discrete samples were measured. However, based on the whole-core data, it is unlikely that any reliable data could be recovered from subsamples.

Site 664

Results from Site 664 are shown in Figures 11 through 13. Archive halves were measured at 3-cm intervals, and several discrete samples were also measured. The low intensity of magnetization precluded shipboard measurement of discrete samples throughout much of the record. Results from our shore-based efforts are presented elsewhere (Valet et al., this volume) and confirm the results discussed here. The sediments below about 30 mbsf were too weak even for our shore-based equipment, which has a noise level of about 5×10^{-12} Am².

This site is located near the equator, and polarity intervals could not be identified from the inclination values. Fortunately, good core recovery meant that all consecutive boundaries were recovered in all three holes. Several cores were also oriented with the multishot tool, which supported our interpretation (see Table 2). The intensity decreases with depth and is just above noise level at about 40 mbsf. No reliable record was obtained below this depth.

Site 665

Paleomagnetic results from Site 665 were an unqualified success. Archive sections measured at 3-cm intervals provided the basis for a high-resolution magnetostratigraphy in sediments too weakly magnetized to measure as discrete samples using the shipboard equipment. As shown in Figures 14 and 15, all major reversal boundaries between the Brunhes and the Gauss were recovered in both holes, allowing the interpretation of the magnetostratigraphic record in the absence of clues from the inclination data. The declination corrections chosen by our usual method were buttressed by core orientation data from the multishot photographic core orientation device (see Table 2). It should be noted that the short normal polarity zones observed below the Jaramillo in both holes cannot be the same subchrons. Correlations facilitated by *P*-wave velocity data clearly preclude this possibility. The intensity records show the familiar pattern of decreasing intensity with increasing depth. Below about 50 mbsf, intensities and inclinations increase dramatically, suggesting a strong and stable vertical overprint probably acquired during coring.

Site 666

Site 666 is noteworthy for the abundance of turbidite sands. These are usually avoided by paleomagnetists in the field owing to their coarse grain size (and associated magnetic instability) as well as to uncertainties about the efficiency of magnetization in such rapidly deposited sediments. Owing to the nature of whole-core measurements, which sample suitable and unsuitable lithologies indiscriminately, we have attempted to edit out data generated by the blind continuous measurement procedure that came from lithologies we would not otherwise sample in the field. Results are shown in Figures 16 (unedited) and 17 (turbidites removed). The data from intervening pelagic units display Type-I behavior and appear to be quite reliable despite the incomplete record.

Polarity determinations were somewhat problematic as no cores were oriented and only two boundaries were contained

Table 2. Comparison of multishot and paleomagnetic declinations (in degrees).

Hole	Core	Multishot	Best guess	Δ	Comments
659A	3H	57-58	50	7	
	4H	230-237	217	13-20	
	5H	70-72	57	13	
	8H	149-150	154	4-5	
	9H 14H-17H				Film ran out Electronic failure
659B	3H	128	—	—	Core not recovered
664C	3H	193	160	33	
	4H	13	—	—	Set pin sheared
	5H	349	311	38	
	6H	150	120	30	
664D	3H	0	340	20	
	4H	162	133	29	
	5H-6H	—	—	—	Exposed film was sent down
665B	2H	270	270	0	
	3H	207	200	7	
	4H	100	100	0	
	5H	329	330	1	
	6H	290	330	40	
	7H	225	350	125	Overprint?
	8H	—	—	—	Core not recovered
	9H	—	—	—	Core disturbed
	668B	3H	153	200	47
4H		20	253	50	

Note: Δ = difference between multishot and best guess.

within a single core. Therefore, declination corrections were determined by relying on demagnetization behavior and biostratigraphic constraints.

Site 667

Results from Site 667 were disappointing (Figs. 18-19). There is no consistent agreement between the whole-core results and the discrete sample data. After correcting the data with multishot declination corrections, there is no clearly identifiable pattern. The highly scattered directions below 30 mbsf do not show any clearly defined reversals. Furthermore, discrete samples were characterized by Type III or IV behavior below about 10 mbsf. We present the data with no interpretation as to polarity.

Site 668

The four cores obtained from Site 668 were processed in the usual manner. The data (Fig. 20) appear to be of exceptional quality; all demagnetization curves were Type I. Core orientations were supported by the multishot tool and agree quite well with biostratigraphic constraints. The B/M boundary and the entire Jaramillo are apparently missing.

CONCLUSION

Reliability of the Multishot Core Orientation Device

We have compiled all of the results from the multishot core orientation device, a photographic record of a magnetic compass attached to the core liner, in Table 2. We also show the "best guess" declination in order to adjust the paleomagnetic data to an average normal declination of zero, as described in the "Methods" section (this chapter). In all but one case, the multishot orientation predicted the correct polarity of the core; we suspect that the paleomagnetic data are overprinted in this particular case.

Although the multishot tool is certainly far from perfect, the polarity of equatorial sites can at least be determined with fair reliability. Such an ability is essential for further work in equatorial regions. Also evident from Table 2 is the unacceptably high degree of failure. Many of the problems encountered could be classified as "avoidable errors," which, with experience, will be eliminated. In general, we found the results to be encouraging.

Utility of Whole-Core Measurements

The shipboard magnetometers are highly reliable instruments. The data produced during Leg 108 were reproduced to a high degree of accuracy in the Scripps Paleomagnetic Laboratory. The utility of such data was limited by two factors: (1) poor paleomagnetic records in the sediments themselves and (2) the inability to remove overprints completely in the 5-mT field available on the pass-through system. The former cannot be remedied, but the latter most certainly can. We cannot overemphasize the importance of acquiring adequate demagnetization capability. Furthermore, the level of demagnetization should not be a matter for curatorial decision making; rather, it should be the responsibility of the shipboard paleomagnetist to determine the proper level of demagnetization of archive sections.

ACKNOWLEDGMENTS

We gratefully acknowledge the invaluable help of the shipboard technical staff. In particular, we wish to thank the paleomagnetic technician, John Tauxe, whose unflagging enthusiasm and expertise were greatly appreciated. We also thank Eunjoo Barg for access to unpublished data on subsamples from "U" channels. Support for this project was provided by Texas A&M University grant #77348 and NSF grant EAR 85-15743.

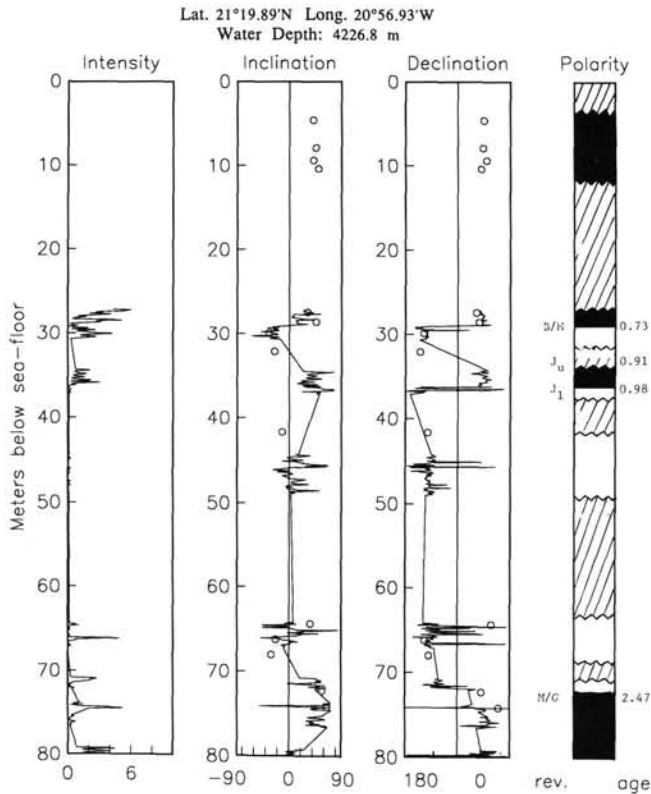


Figure 3. Magnetostratigraphic results from Hole 657B. Intensity units are 10^{-2} Am², as explained in the "Methods" section, this chapter. Lines are data from entire cores or archive halves, as discussed in the text. Circles are discrete sample data. All polarity zones longer than 20 cm are indicated in the polarity logs. Gaps are shown as hachured areas, normal zones are black, and reversed zones are white. Boundaries delineated with a ragged (straight) line lie between (within) cores. Reversal boundaries are marked with the following conventions: Brunhes/Matuyama (B/M), upper and lower Jaramillo (J_u and J_l , respectively), upper and lower Olduvai (O_u and O_l respectively), Matuyama/Gauss (M/Ga), and Gauss/Gilbert (Ga/Gi). The ages (Ma) are those of Berggren et al. (1985).

REFERENCES

Berggren, W. A., Kent, D. V., Flynn, J. J., and Van Couvering, J. A., 1985. Cenozoic geochronology. *Geol. Soc. Am. Bull.*, 96: 1407-1418.

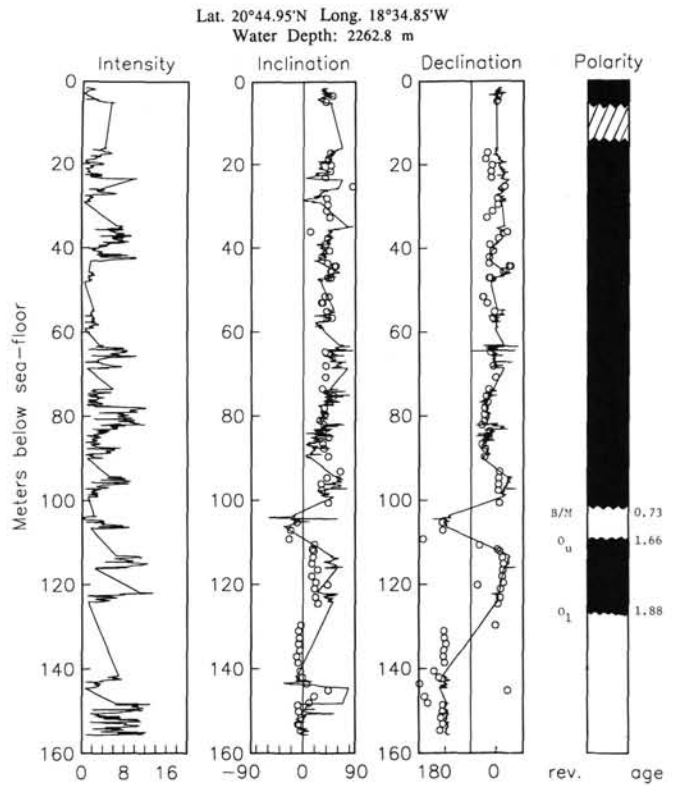


Figure 4. Magnetostratigraphic results from Hole 658A. See Figure 3 caption for an explanation of the symbols and abbreviations used.

Hays, J. D., Saito, T., Opdyke, N. D., and Burckle, L. H., 1969. Pliocene-Pleistocene sediments of the equatorial Pacific: their paleomagnetic, biostratigraphic, and climatic record. *Geol. Soc. Am. Bull.*, 80:1481-1513.

Opdyke, N. D., Burckle, L., and Todd, A., 1974. The extension of the magnetic time scale in sediments of the Central Pacific Ocean. *Earth Planet. Sci. Lett.*, 22:300-306.

Theyer, F., and Hammond, S. R., 1974. Cenozoic magnetic time scale in deep-sea cores: completion of the Neogene. *Geology*, 2:487-492.

Date of initial receipt: 21 March 1988
Date of acceptance: 3 August 1988
Ms 108B-154

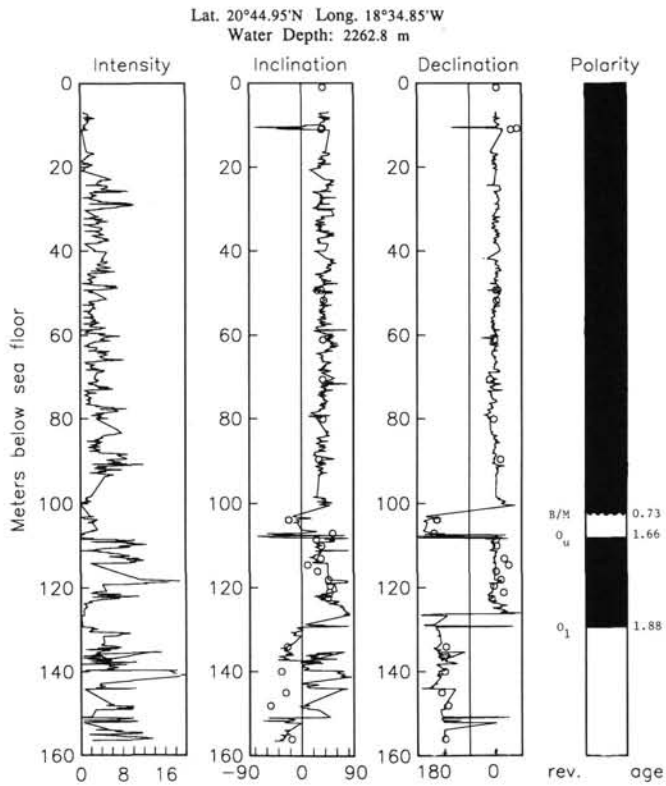


Figure 5. Magnetostratigraphic results from Hole 658B. See Figure 3 caption for an explanation of the symbols and abbreviations used.

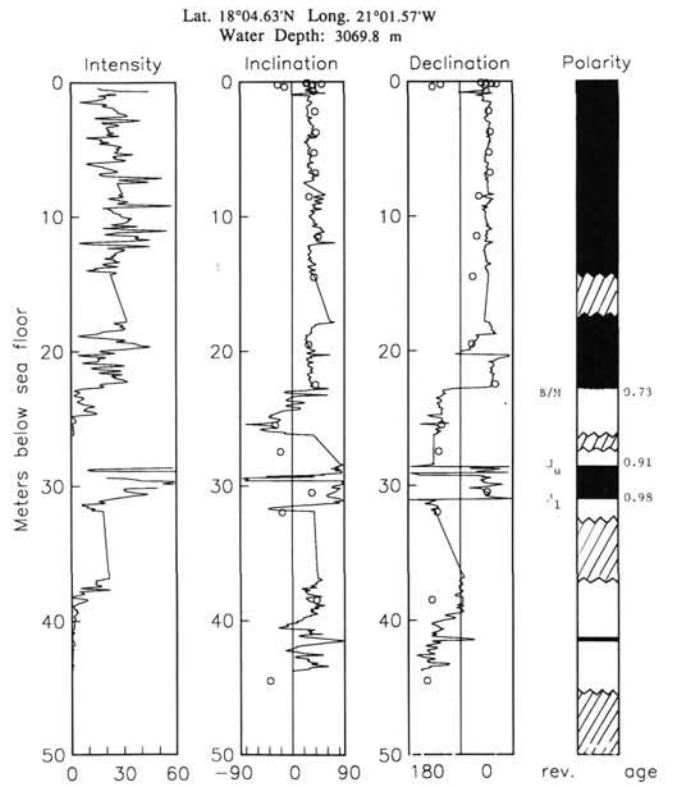


Figure 6. Magnetostratigraphic results from Hole 659A. See Figure 3 caption for an explanation of the symbols and abbreviations used.

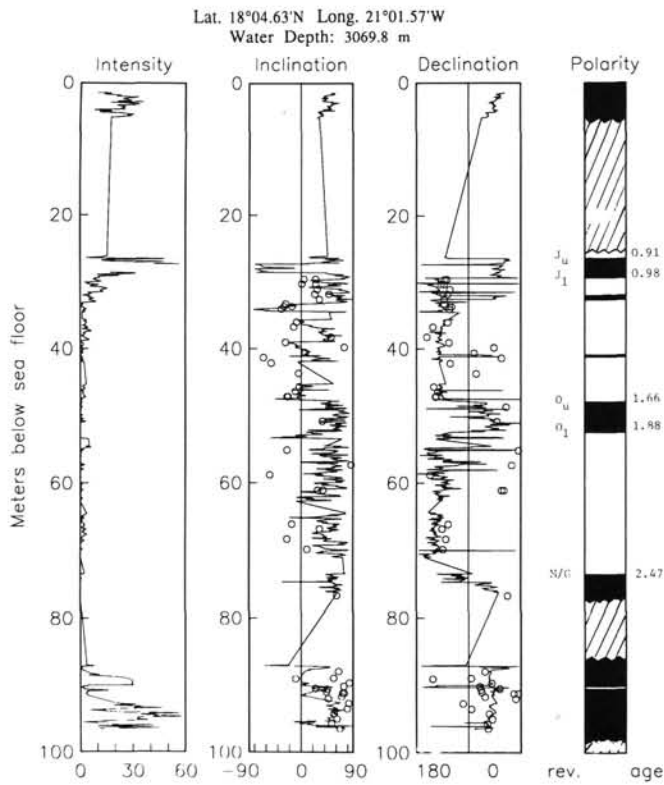


Figure 7. Magnetostratigraphic results from Hole 659B. See Figure 3 caption for an explanation of the symbols and abbreviations used.

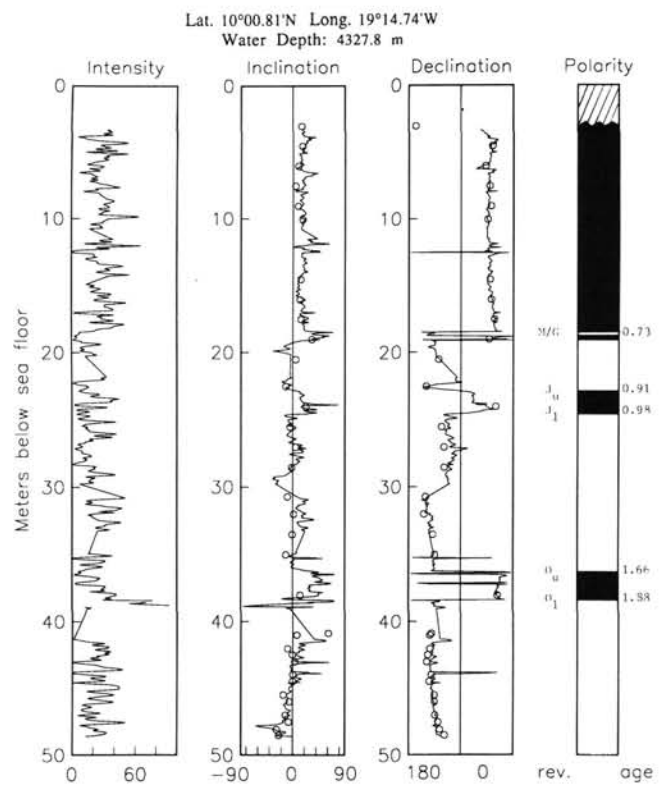


Figure 8. Magnetostratigraphic results from Hole 660A. See Figure 3 caption for an explanation of the symbols and abbreviations used.

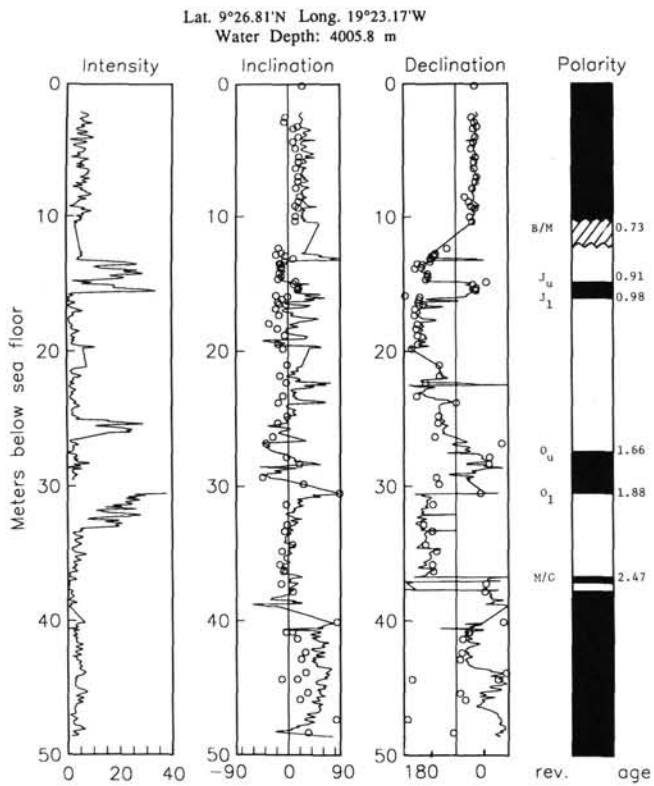


Figure 9. Magnetostratigraphic results from Hole 661A. See Figure 3 caption for an explanation of the symbols and abbreviations used.

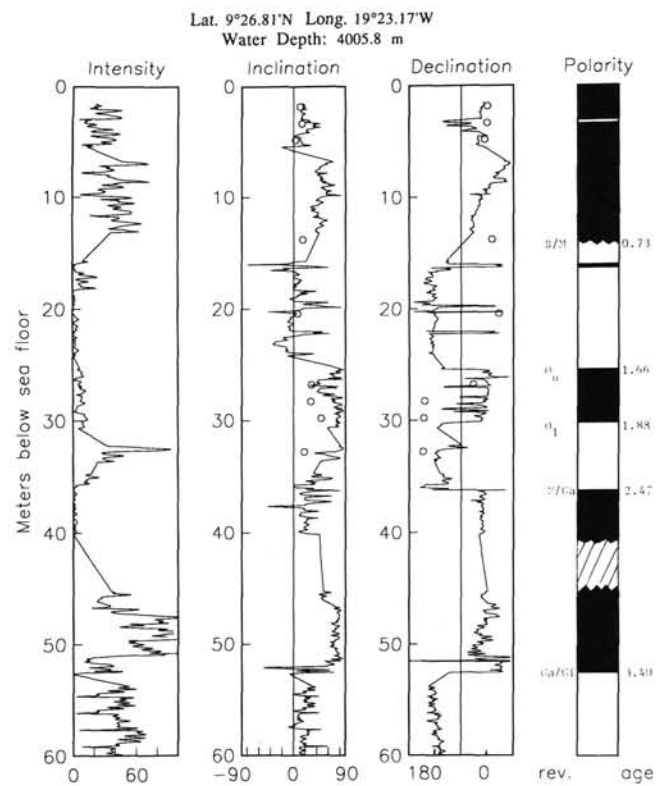


Figure 10. Magnetostratigraphic results from Hole 661B. See Figure 3 caption for an explanation of the symbols and abbreviations used.

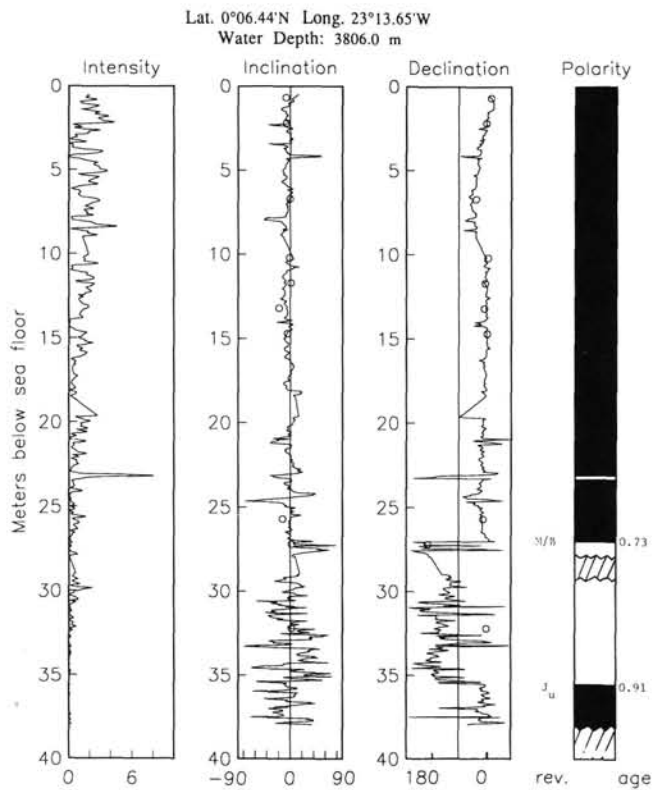


Figure 11. Magnetostratigraphic results from Hole 664B. See Figure 3 caption for an explanation of the symbols and abbreviations used.

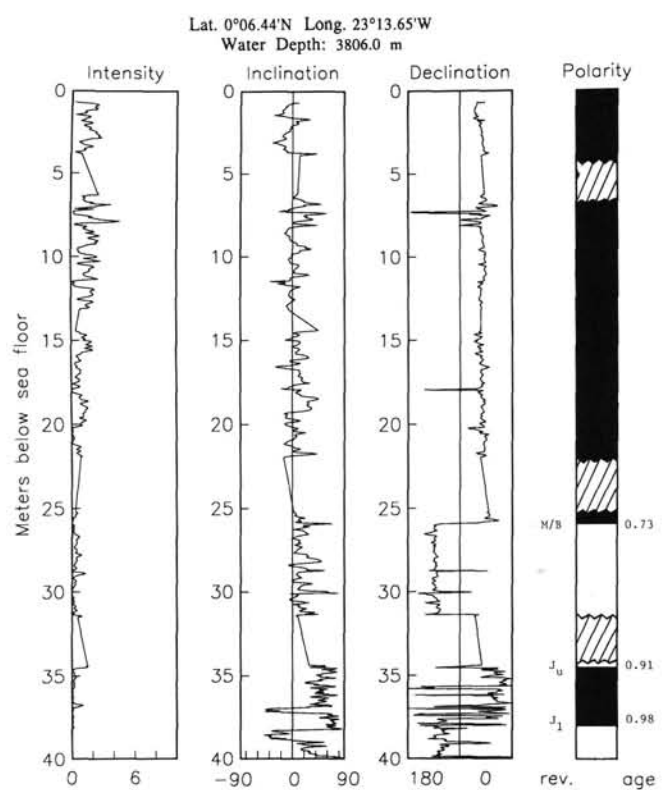


Figure 12. Magnetostratigraphic results from Hole 664C. See Figure 3 caption for an explanation of the symbols and abbreviations used.

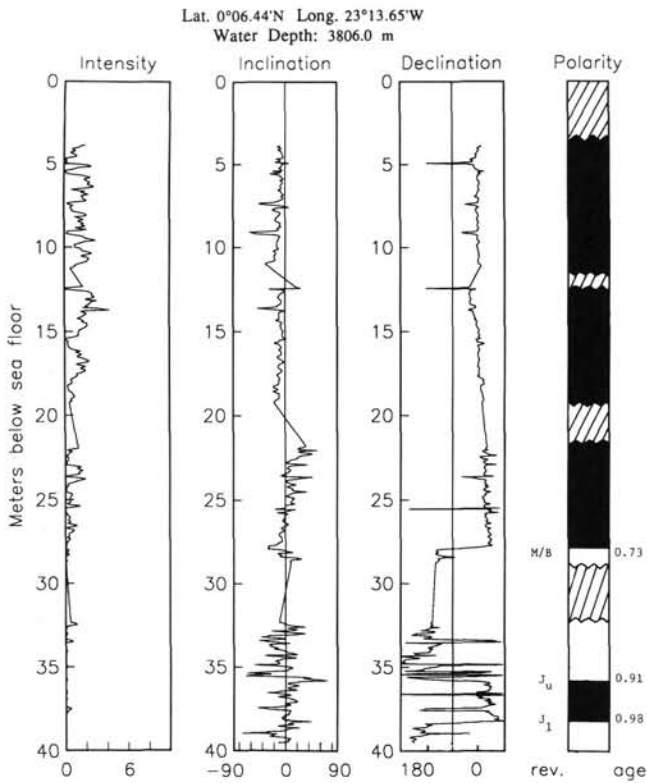


Figure 13. Magnetostratigraphic results from Hole 664D. See Figure 3 caption for an explanation of the symbols and abbreviations used.

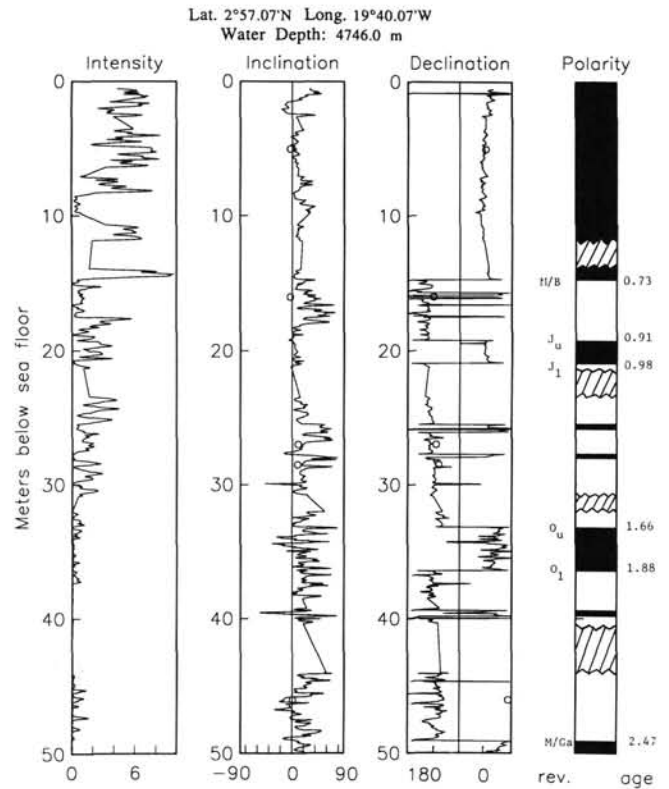


Figure 14. Magnetostratigraphic results from Hole 665A. See Figure 3 caption for an explanation of the symbols and abbreviations used.

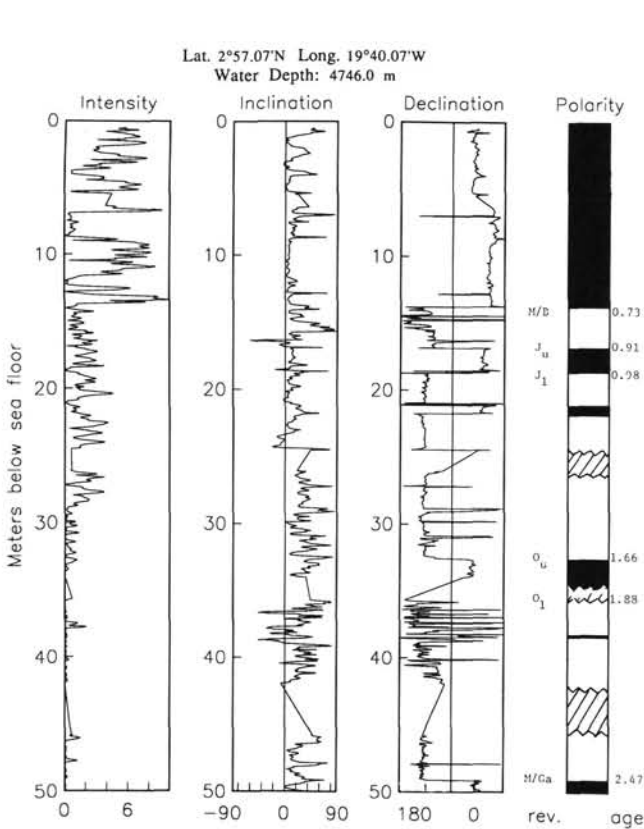


Figure 15. Magnetostratigraphic results from Hole 665B. See Figure 3 caption for an explanation of the symbols and abbreviations used.

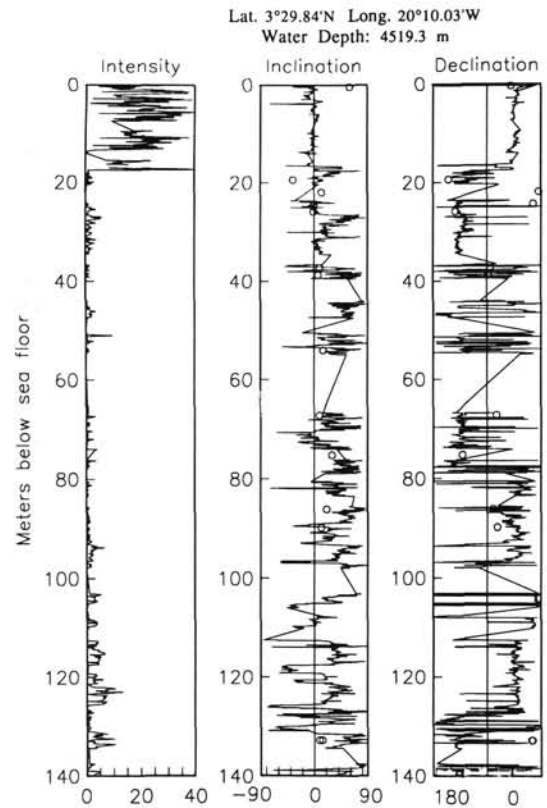


Figure 16. Magnetostratigraphic results from Hole 666A. See Figure 3 caption for an explanation of the symbols and abbreviations used.

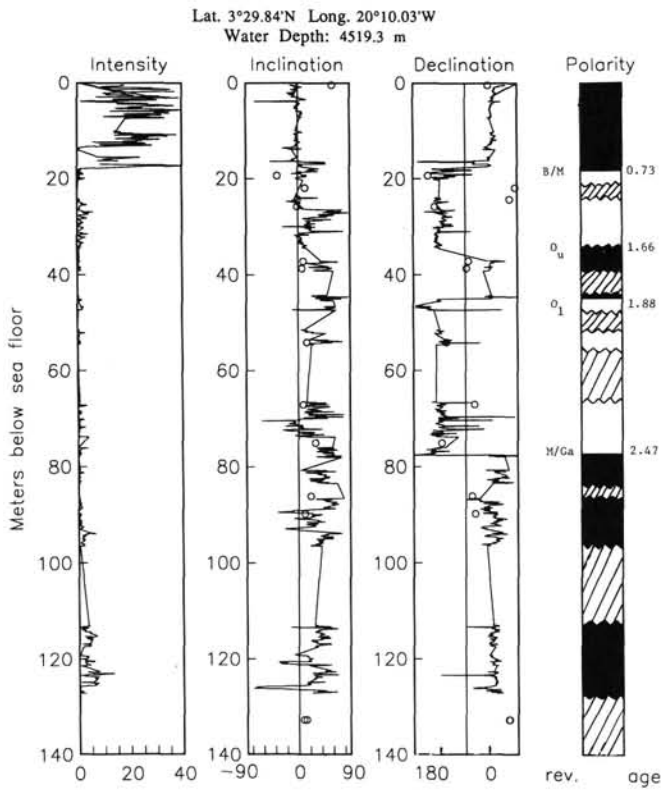


Figure 17. Magnetostratigraphic results from Hole 666A (turbidites removed). See Figure 3 caption for an explanation of the symbols and abbreviations used.

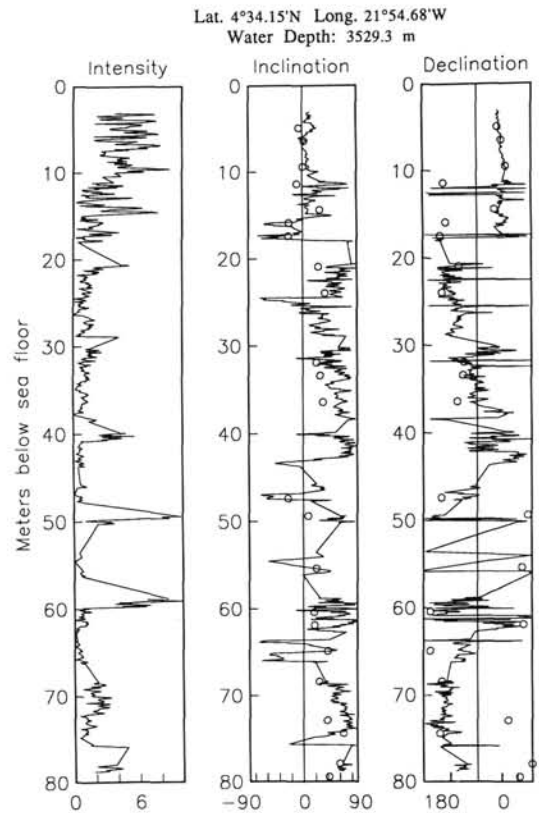


Figure 18. Magnetostratigraphic results from Hole 667A. See Figure 3 caption for an explanation of the symbols and abbreviations used.

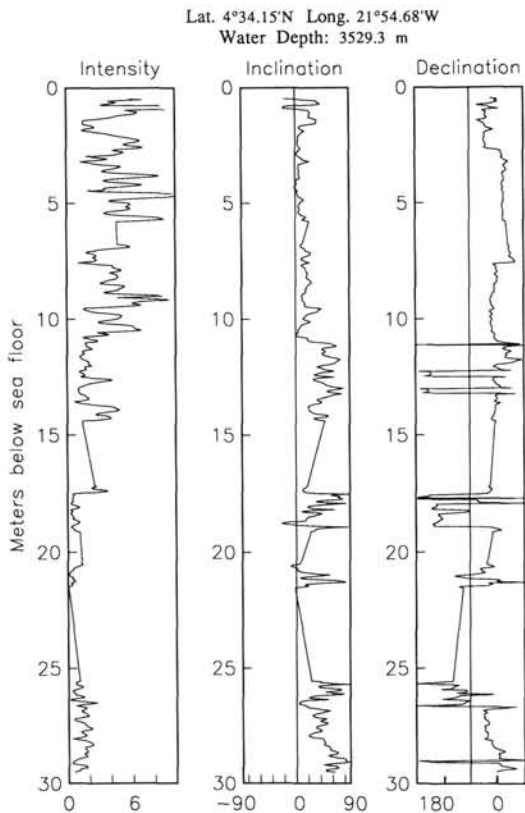


Figure 19. Magnetostratigraphic results from Hole 667B. See Figure 3 caption for an explanation of the symbols and abbreviations used.

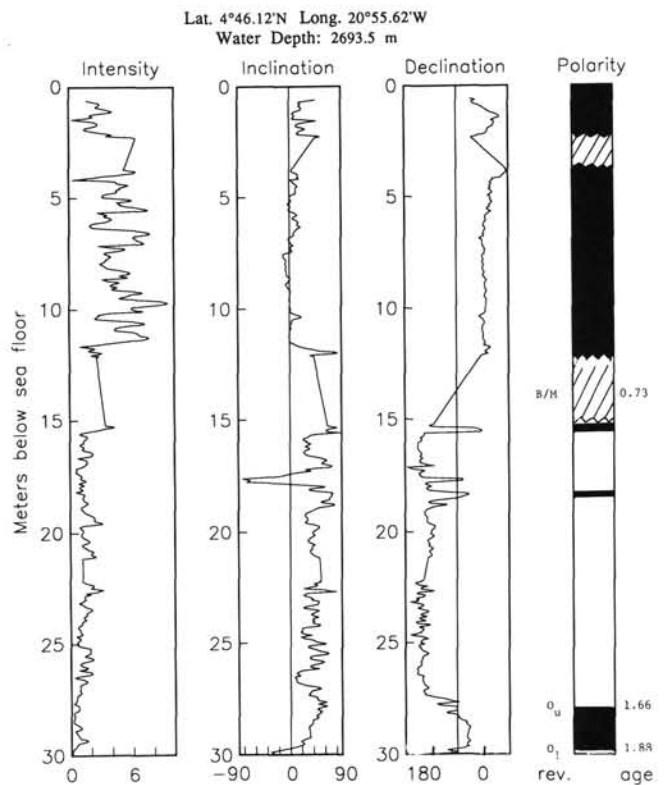


Figure 20. Magnetostratigraphic results from Hole 668B. See Figure 3 caption for an explanation of the symbols and abbreviations used.